sciendo
Power Electronics and Drives
Volume 8(43), 2023 DOI: 10.2478/pead-2023-0008

Simulation Time Reduction with 2.5D FEM Analysis for Axial Flux Machines

Research paper

Mike Königs*, Haithem Baccouche, Steffen Breser, Tobias Jöns, Bernd Löhlein

Chair of Electrical Drive System Development, Flensburg University of Applied Sciences, Flensburg, Germany

Received: January 8, 2023; Accepted: March 6, 2023

Abstract: In this paper, an approach for a two-and-half-dimensional (2.5D) finite element method (FEM)-based analysis, or quasi-three-dimensional (3D) FEM analysis, of an axial flux machine is discussed. By cutting the 3D model laterally and thereby creating cylindrical surface cuts, the 3D model can be split into several cylindrical surfaces. Transforming those cylindrical cuts into planes leads to a layer-based two-dimensional (2D) model with different radii for each layer. By integrating over all lateral surface cuts, the results for the entire axial flux machine can be determined. In comparison to the simulation of a full 3D FEM model, the simulation of the proposed 2.5D model is much faster. To validate the approach, the two main types of axial flux machines are simulated with both 3D-FEM-based model and 2.5D-FEM-based approach, and the results are presented in this paper.

Keywords: *axial flux machine • FEM analysis • model reduction • 2.5D FEM • quasi-three-dimensional FEM*

1. Introduction

Axial flux machines (AFMs) have experienced a major surge of interest in the industry over the past couple of years. This is especially true in the automotive industry. The characteristic of the standard AFM, as a machine with concentrated winding, facilitates its manufacture. In addition, its increased torque density compared to conventional radial flux machines (RFMs) is a benefit. However, regarding the design process, so far most engineers have utilised three-dimensional (3D) finite element method (FEM) analyses (e.g. Ishikawa, 2015; Simon-Sempere et al., 2021), which come at the cost of increased computation times and hardware requirements (Loehlein, 2019). Model reduction methods are, therefore, of exceptional importance, as stated by Dedden (2012) and by COMSOL, the developer of Multiphysics FEM software, on their web page '*Using Symmetry to Reduce Model Size*' (accessed: 18.01.2023). For conventional RFMs, the issue is mitigated by utilising two-dimensional (2D) FEM simulations, which are significantly faster (Ponomarev et al. 2016; van der Giet et al., 2008). This is rather precise for RFMs because RFMs can, most of the time, be generated by extruding a single 2D-sheet geometry. For AFMs, no such extrusion plane exists. However, various attempts to establish 2D models have been made. Lubin et al. (2013) have used a translational system for the analytic modelling of an axial-field magnetic gear. Egea et al. (2010) utilise a combination of 2D FEM analysis and an analytical approach. Gołębioeski (2018) and Smoleń (2018) have used an algorithm to numerically solve AFMs based on a 2D model in several publications. Guo et al. (2022) have developed a procedure to transform AFMs into a conventional RFM topology. In 2004, Parviainen et al. started the first attempts to model AFMs in two dimensions. The models utilised for the 2D simulations can be expanded into two-and-half-dimensional (2.5D) FEM simulations. For certain variants of AFMs, these quasi-3D FEM analyses have been conducted earlier. Hameida et al. (2019) modelled a yokeless and segmented armature (YASA)-type AFM in a 2D multi-slice model. Gulec and Aydin (2017) limited their investigation to the analysis of a torus-type double-rotor AFM, while Kim and Woo (2022) applied the idea to a single-rotor single-stator topology. Multiple AFM topologies were reviewed by Hao et al. (2022). In this article, focus will be placed on two common types of AFMs, namely the single-rotor double-stator I-type topology and the double-rotor single-stator H-type (YASA) topology.

* *Email: mike.koenigs@hs-flensburg.de*

This paper investigates whether a 2.5D FEM simulation of AFMs is feasible for both types of machines and whether a significant computational advantage is obtained.

2. Simulation Setup

2.1. Software and hardware

The analysis was performed using Ansys Electronics Desktop Maxwell 3D R2021 (Ansys: ANSYS, Inc., 275 Technology Drive, Canonsburg, PA 15317). A transient simulation utilising a quadratic solution approach was conducted. The computation was conducted on a Fujitsu Celsius M7010N (Fujitsu: Fujitsu Technology Solutions GmbHMies-van-der-Rohe-Straße 880807 Munich Germany) workstation with an Intel Xeon W-2235 central processing unit (CPU) and 32 GB of random access memory (RAM).

2.2. Geometry

Two different geometries will be studied to validate a 2.5D calculation approach for AFMs. The two most prevalent cases of AFMs are H-type machines with two coupled rotors and one stator, also known as YASA (Figure 1: right illustration), and I-type machines with one rotor and two stator components on each side of the rotor (Figure 1: left illustration). Both typologies will be subject to research in this publication. Both topologies will utilise concentrated windings. Topologies with concentrated windings, due to their easier manufacturability, represent the majority of AFM designs. Machine 1 will utilise the I-topology with 10 poles and 12 slots. Machine 2 will utilise the H-topology with 16 poles and 18 slots. The machine parameters are shown in Table 1. The ferromagnetic material is modelled

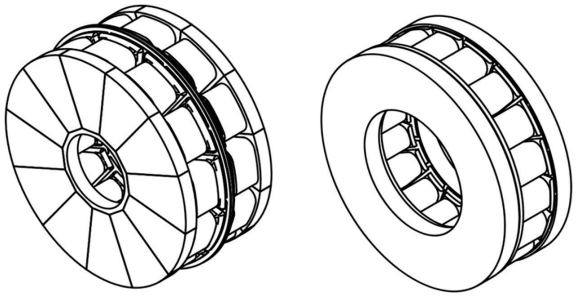

Fig. 1. Investigated topologies: I-type is on the left, and H-type is on the right.

Attribute	Machine 1	Machine 2
Type	I-type	H-type (YASA)
Number of poles	10	16
Number of slots	12	18
Winding type	Concentrated double-layer winding	Concentrated double-layer winding
Outer diameter of rotor (mm)	260	255
Inner diameter of rotor (mm)	70	135
Air gap width (mm)	2	1
Magnet thickness (mm)	5	5
Rotor yoke thickness (mm)	-	15
Outer diameter of stator (mm)	250	255
Inner diameter of stator (mm)	80	140
Axial length of stator (mm)	55	50
Stator yoke thickness (mm)	15	-
Yoke material	AISI 1008	AISI 1008
Axial length of machine (mm)	120	95

AISI, American Iron and Steel Institute; YASA, yokeless and segmented armature.

Table 1. Machine parameters.

as a non-linear material, and saturation effects will occur. The permanent magnets have the grade N35 and are represented by a linear model in the working point. All conductors are defined as stranded conductors. Therefore, no current displacement effects will be considered in the windings.

3. Two-and-Half-Dimensional Simulation of AFMs

3.1. Basic principle

With regard to the simulation of RFMs, 2D FEM simulations are the ordinary simulation domain. Rarely, 3D simulations are conducted when the need for the representation of special edge effects is given. Due to the axial extrusion characteristic of RFMs, the 2D simulation of an axial sectional view is often sufficient. Skew effects can be modelled by using 2.5D simulation techniques. For AFMs, no such extrusion characteristic of a sectional view exists. Therefore, 3D simulations are required. However, under further investigation, a mathematical description for radial sections of lateral surfaces can be derived. The lateral surface can then be transformed into a 2D plane. To calculate the system characteristics, multiple lateral sectional surface cuts will be generated. Figure 2 displays an example of lateral surface cuts.

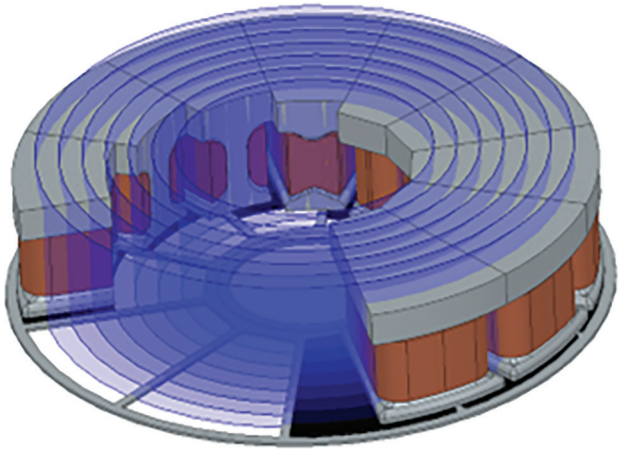

Fig. 2. Lateral surface cuts in an I-type axial flux machine.

3.2. Two-dimensional lateral surface cuts

The lateral surface cuts, which are still 3D entities, can now be transformed into 2D structures. This is done by cutting the lateral surface and transforming the cylindrical surface into a plane (Figure 3). The physical connection of the sides of planes A and B can be added to the numerical simulation by defining dependent and independent boundary conditions, respectively. The formerly rotational motion $\vec{\omega}$ of the AFM has now equivalently been transformed into a translational motion $\vec{v}$.

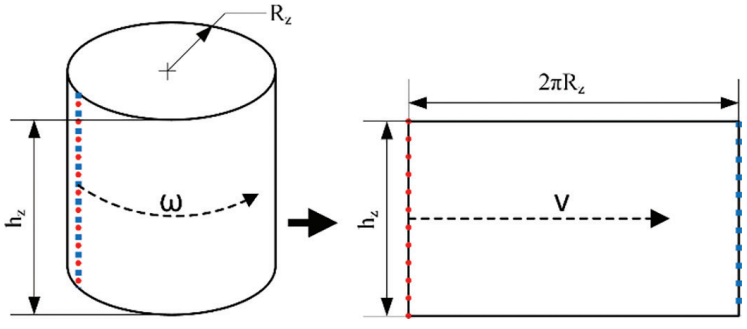

Fig. 3. Geometry transformation from 3D to 2D.

For most designs, mathematical equations for the 2D lateral surface cuts can be found. The radius of the lateral surface cut can be parameterised to automatically alter the geometry used for the 2.5D FEM simulation. Examples of a variety of radii for the three lateral surface cuts can be found in Figure 4.

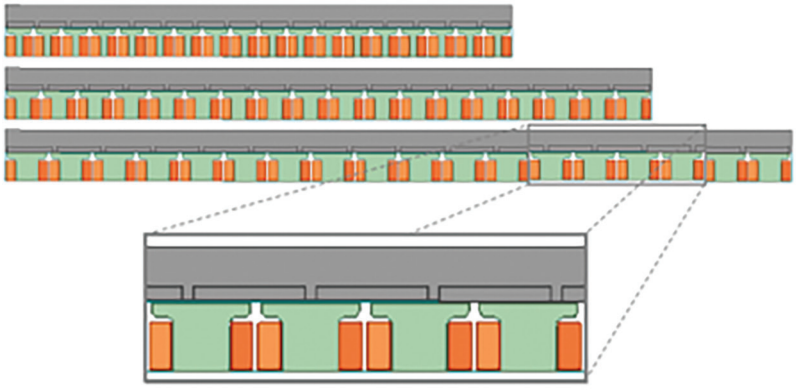

Fig. 4. Two-dimensional simulation cuts: H-type.

The discrete integration of all lateral surface cuts (in this case, rectangular integration) from the inner radius of the machine to the outer radius of the machine then yields the results, which will be compared to the results of 3D simulation. In both cases (Figures 2 and 4), a symmetry boundary condition in the axial symmetry plane is applied in order to cut the model size in half.

4. Results

4.1. Required computation time

As follows, 2.5D simulations can significantly reduce computation time. Table 2 shows the calculation times for both motors in the load and no-load cases for both 2.5D simulations and 3D simulations. For M1, there are two 2.5D simulations, one with eight lateral surface cuts and one with 16 lateral surface cuts. The 2.5D simulation of M2 facilitates 20 lateral surface cuts. A coarse lateral surface cut can decrease the computation time in the no-load case of M1 from 45 h of the 3D simulation to just more than 30 min, while the finer lateral surface cuts result in a simulation time of just >1 h. This represents a computation time of 2.66% of the 3D simulation. An even better reduction of computation time can be achieved in the load case. In the case of M2, the increased number of lateral surface cuts and mesh operations limit the calculation time reduced by a factor of 20. The scalar potential definitions, numerical element descriptions and numbers of elements are given in Table 3.

Experimental condition	Time (h:m:s)	Percentage
M1 3D no-load condition	44:50:13	
M1 2.5D no-load condition	0:35:20	1.31
M1 2.5D fine no-load condition	1:11:36	2.66
M1 3D load condition	64:31:26	
M1 2.5D load condition	0:35:27	0.92
M1 2.5D fine load condition	1:10:45	1.83
M2 3D no-load condition	110:4:52	
M2 2.5D no-load condition	5:39:7	5.13
M2 3D load condition	122:21:13	
M2 2.5D load condition	5:25:15	4.43

Table 2. Computation times.

	M1	M2
3D Number of elements	1,617,000	961,000
3D Element description	Tetrahedron	Tetrahedron
3D Scalar potential definition	Quadratic	Quadratic
2D Number of elements	~65,000 per slice	~11,000 per slice
2D Element description	Triangle	Triangle
2D Scalar potential definition	Linear	Linear

Table 3. Mesh statistics.

4.2. Machine 1

4.2.1. No-load condition

At first, the results for M1 under no-load conditions are presented. Figure 5 shows the induced voltage under the no-load condition for the 3D FEM and both 2.5D simulations. Both 2.5D simulations yield results comparable to the 3D simulation. A numerical ripple can be observed in the 3D simulation. A significantly increased amount of mesh elements is likely to suppress the numerical ripple. However, a larger amount of mesh elements would increase the computation time even further. The Fourier transform of the induced voltage is shown on the right side of Figure 5. Similar harmonic components are present, and the 2.5D and the 3D analyses match well.

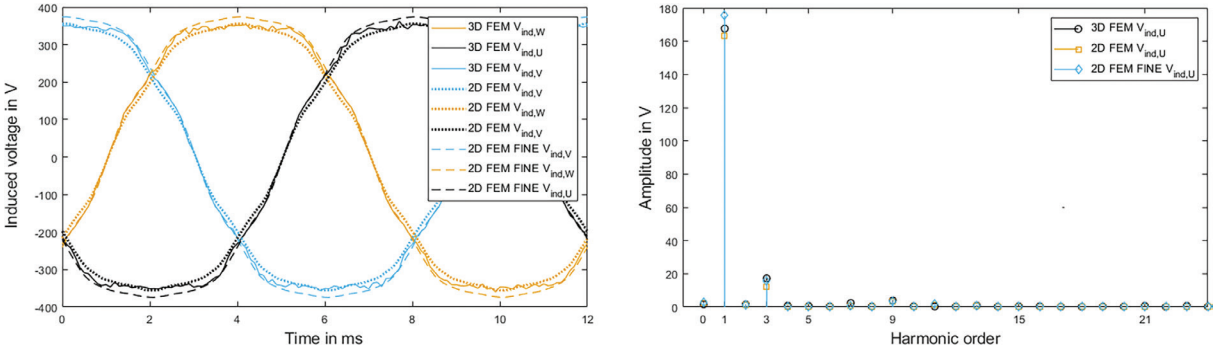

Fig. 5. M1: Induced voltage under no-load condition. FEM, finite element method with 16 lateral surface cuts.

Cogging torque is an important factor in machine design. Even under no-load conditions, cogging torque can significantly contribute to noise, vibration and harshness (NVH). The cogging torque of M1 is shown in Figure 6. It can be observed that the cogging torque in the 3D simulation has half the amplitude of the cogging torque in the 2.5D simulations. The discrete Fourier transform of the 2.5D cogging torque displays the same harmonics as the 3D simulation.

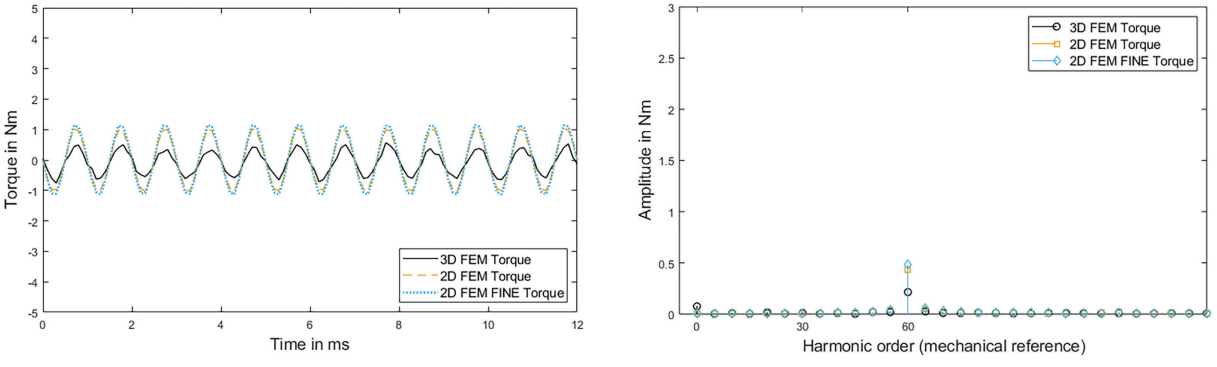

Fig. 6. M1: Torque ripple under no-load condition. FEM, finite element method with 16 lateral surface cuts.

4.2.2. Load condition

For the load condition, a sinusoidal current of 5 A was impressed into the machine winding. Figure 7 shows the induced voltage under the load case. Again, a good agreement between the simulation methods can be observed. Additional harmonics can be observed due to saturation effects. This also holds true for the discrete Fourier transform of the induced voltage, even though the base harmonic is slightly reduced in the coarse 2.5D simulation.

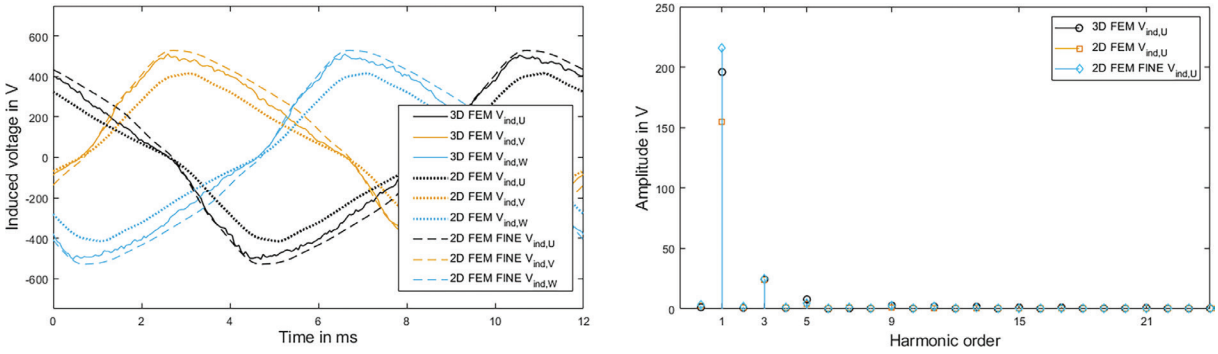

Fig. 7. M1: Induced voltage under load condition. FEM, finite element method with 16 lateral surface cuts.

The torque of M1 in this load scenario is in between the coarse number of lateral surface cuts and the finer scenario (Figure 8). The finer scenario shows an increased torque compared to the 3D simulation. This is likely due to saturation effects, which cannot, in the case of AFM with overhanging teeth, be modelled in 2D as accurately as in 3D.

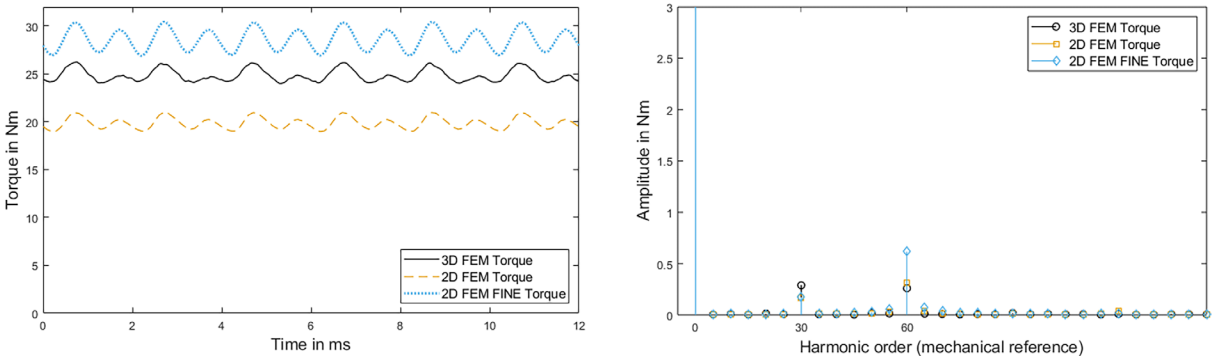

Fig. 8. M1: Torque under load condition. FEM, finite element method with 16 lateral surface cuts.

Again, the results for the fast Fourier transform (FFT) of the signals agree well in terms of observable harmonic orders. Other than the DC part of the torque, ripples of the sixth and 12th harmonic order are observable. This coincides with the cogging torque of the machine.

4.3. Machine 2

4.3.1. No-load condition

In this section, the results for M2 are discussed. Like M1, a no-load condition and a load condition are discussed. Similar to M1, both the FFT and the time signal of the induced voltage in the no-load case match well under all simulation methods (Figure 9). Again, a numerical ripple can be observed in the induced voltage of the 3D FEM simulation. In reality, a smother induced voltage curve is prevalent.

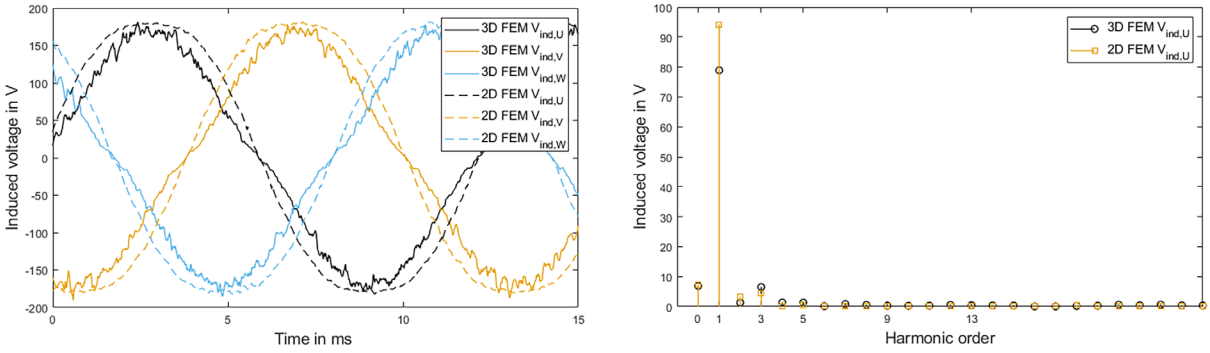

Fig. 9. M2: Induced voltage under no-load condition. FEM, finite element method.

The torque ripple, however, does not match as well as was the case in M1 (Figure 10). A numerical ripple with few mesh nodes and interpolation effects is likely the cause for this effect. This assumption is further strengthened by the frequency spectrum given in Figure 10 on the right side. The 2.5D simulation yields the expected frequency of the current ripple based on the slot/pole combination, which is not observable in the 3D simulation. This is likely due to meshing effects.

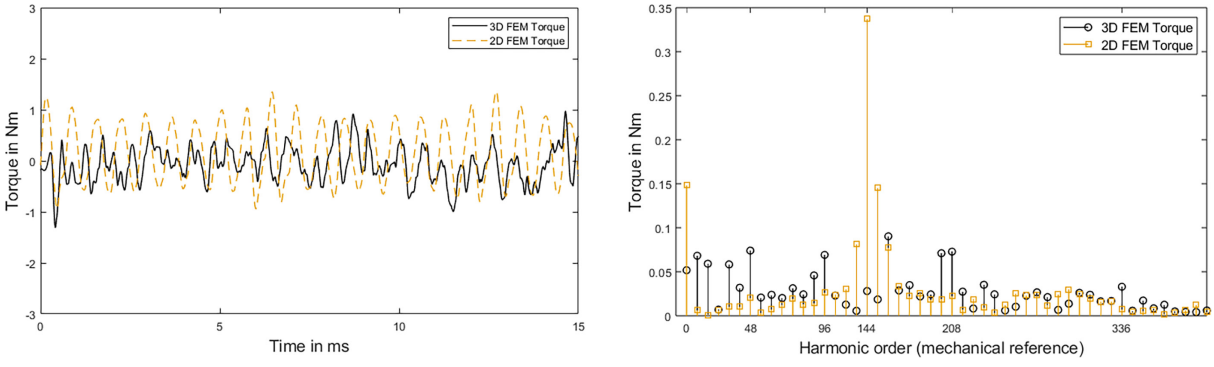

Fig. 10. M2: Torque ripple under no-load condition. FEM, finite element method.

4.3.2. Load condition

Under load conditions, the induced voltage shows a good agreement again between both methods, in the time domain as well as in the frequency domain (Figure 11). Not only do the amplitudes match, but the frequency components also match well. Again, saturation effects are observable.

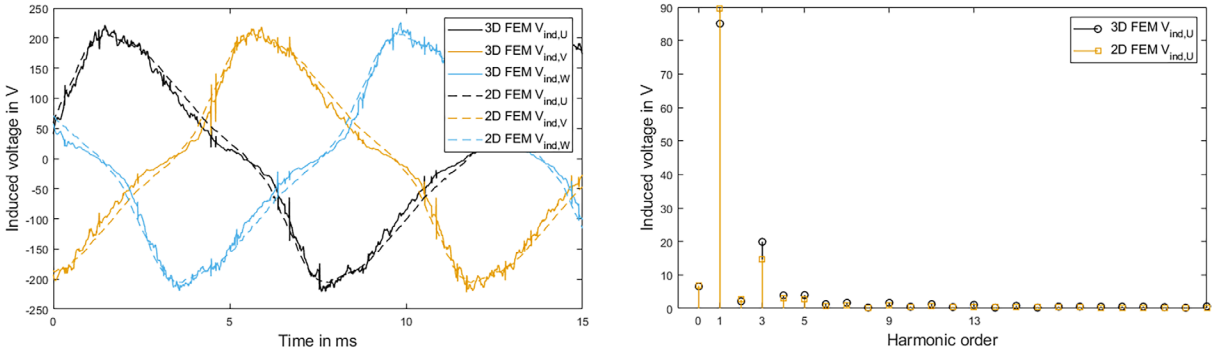

Fig. 11. M2: Induced voltage under load condition. FEM, finite element method.

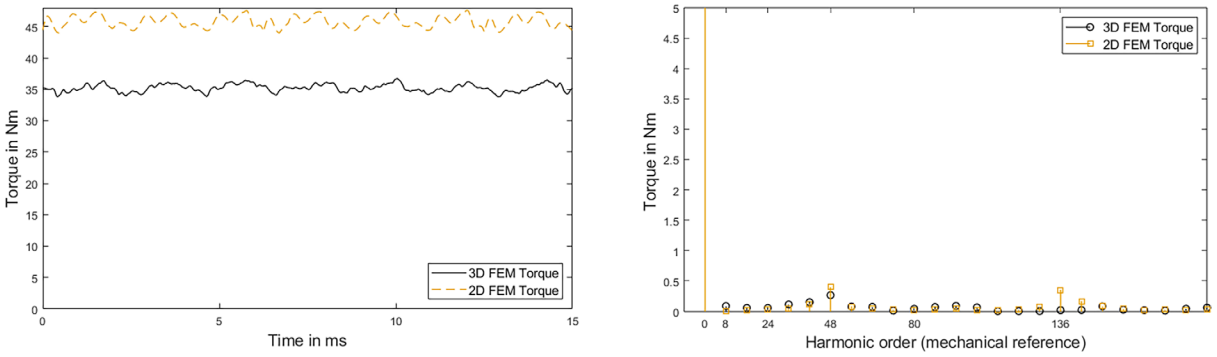

Fig. 12. M2: Torque under load condition. FEM, finite element method.

The torque in the 3D simulation is much lower than the torque in the 2.5D simulation, again likely due to saturation effects (Figure 12). Further research needs to be conducted. Since the induced voltage is quite similar in both simulation cases, we would have expected a similar torque when the coils are exposed to identical currents. The torques and forces are calculated in Ansys Maxwell by using the virtual workforce principle. It is possible that different methods, e.g. Lorentz force calculations or use of the Maxwell stress tensor, will alleviate this issue. Further research is needed to prove these hypotheses.

5. Viability of 2.5D Simulations for AFMs

It has been shown that all 2.5D simulations show good agreement in terms of the induced voltage. The results for torques, however, are inaccurate. This can be due to interpolation errors, saturation effects or the amount of mesh used for the discretisation. However, a large number of effects important for machine design can be accounted for in 2.5D simulations. Furthermore, a significant reduction in calculation time can be achieved, which enables the use of enhanced optimisation algorithms in the machine design process. Therefore, 2.5D simulations can be an important tool in the design process of AFM.

6. Summary

This paper investigates the feasibility and advantages of 2.5D FEM simulations of AFMs. The 3D model can be divided into a variable number of cylindrical 3D objects using cylindrical cuts. The surface of these cylindrical objects can be transformed into a 2D plane, resulting in a 2D layer-based model. The result of the 2.5D FEM is obtained by integrating the results through different layers. This paper shows the simulation results for the H-type and I-type of AFMs in comparison to the 3D FEM simulation.

For comparison, both machines are simulated under no-load and load conditions. The H-type is modelled with eight and 16 lateral surface cuts and the I-type with 20 lateral surface cuts. Under no-load conditions, the computation time of the 3D FEM needs about 45 h, which can be decreased to 35 min (1.31%) by using the 2.5D FEM simulation with eight layers. Doubling the number to 16 layers also doubles the computing time. A better reduction can be achieved in the load case, wherein the computation time of the 3D FEM increases and the computation time of the 2.5D FEM stays the same. Similar results are obtained for the I-type. Furthermore, the induced voltages and torque characteristics are compared. The induced voltages and their harmonics show good agreement for both machine types. The torque of both machines is inaccurate; while the harmonics of the H-type match well, the harmonics of the I-type do not. This is probably due to interpolation errors, saturation effects or the element number of the mesh. Regarding the inverter-related phenomenon, however, 2.5D FEM analysis offers the opportunity to directly couple the multi-slice model to a power electronics model in order to perform a co-simulation of the system. This is not feasible with conventional 3D FEM simulations of AFMs due to computation time deficits.

References

Dedden, R. (2012). *Model Order Reduction using the Discrete Empirical Interpolation Method | TU Delft Repositories*. Available at: https://repository.tudelft.nl/islandora/object/uuid:6f1531d7-a956-4c70-b8af-149111a9243d. (Last accessed on March 3rd 2023).

Egea, A., Almandoz, G., Poza, J. and Gonzalez, A. (2010). Axial flux machines modelling with the combination of 2D FEM and analytic tools. In: *The XIX International Conference on Electrical Machines – ICEM 2010* [Preprint]. Available at: https://doi.org/10.1109/icelmach.2010.5608115.

Gołębiowski, M. (2018). *Functional simulation model of the axial flux permanent magnet generator – Archives of Electrical Engineering – PAS Journals*. Available at: https://journals.pan.pl/dlibra/publication/124745/edition/108845/content. (Last accessed on March 3rd 2023).

Gulec, M. and Aydin, M. (2017). Implementation of Different 2D Finite Element Modelling Approaches in Axial Flux Permanent Magnet Disc Machines." *IET Electric Power Applications*, 12(2), pp. 195–202. Available at: https://doi.org/10.1049/iet-epa.2017.0434.

Guo, B., Peng, F., Khedda, D. Z., Dubas, F. and Huang, Y. (2022). Transformation between Axial- and Radial- Flux Permanent-Magnet Machines. *IEEE Transactions on Transportation Electrification*, pp. 1–1. Available at: https://doi.org/10.1109/tte.2022.3218792.

Hao, Z. (2022). *A Review of Axial-Flux Permanent-Magnet Motors: Topological Structures, Design, Optimization and Control Techniques*. Available at: https://www.mdpi.com/2075-1702/10/12/1178.

Hemeida, A., Lehikoinen, A., Rasilo, P., Vansompel, H., Belahcen, A., Arkkio, A. and Sergeant, P. (2019). A Simple and Efficient Quasi-3D Magnetic Equivalent Circuit for Surface Axial Flux Permanent Magnet Synchronous Machines. *IEEE Transactions on Industrial Electronics*, 66(11), pp. 8318–8333. Available at: https://doi.org/10.1109/tie.2018.2884212.

Ishikawa, T. (2015). Design of an axial-flux type permanent-magnet generator. *2015 IEEE Magnetics Conference (INTERMAG).* [Preprint]. Available at: https://doi.org/10.1109/intmag.2015.7157417.

Kim, K. H. and Woo, D. K. (2022). Novel Quasi-Three-Dimensional Modeling of Axial Flux In-Wheel Motor With Permanent Magnet Skew. *IEEE Access*, 10, pp. 98842–98854. Available at: https://doi.org/10.1109/access.2022.3206774.

Löhlein, B. (2019). *Mechatronische Antriebssysteme mit PM-Synchronmaschinen und ihr Entwurf*. Shaker Verlag. https://www.shaker.de/de/content/catalogue/index.asp?lang=de&ID=8&ISBN=978-3-8440-8144-2&search=yes ISBN: 978-3-8440-8144-2

Lubin, T., Mezani, S. and Rezzoug, A. (2013). Development of a 2-D Analytical Model for the Electromagnetic Computation of Axial-Field Magnetic Gears. *IEEE Transactions on Magnetics*, 49(11), pp. 5507–5521. Available at: https://doi.org/10.1109/tmag.2013.2267746.

Parviainen, A., Niemela, M. and Pyrhonen, J. (2004). Modeling of Axial Flux Permanent-Magnet Machines. *IEEE Transactions on Industry Applications*, 40(5), pp. 1333–1340. Available at: https://doi.org/10.1109/tia.2004.834086.

Ponomarev, P., Keränen, J., Lyly, M., Westerlund, J. and Råback, P. (2016). Multi-slice 2.5D modelling and validation of skewed electrical machines using open-source tools. In: *2016 IEEE Conference on Electromagnetic Field Computation (CEFC)* [Preprint]. Available at: https://doi.org/10.1109/cefc.2016.7815918.

Simon-Sempere, V., Simón-Gómez, A., Burgos-Payán, M. and Cerquides-Bueno, J. R. (2021). Optimisation of Magnet Shape for Cogging Torque Reduction in Axial-Flux Permanent-Magnet Motors. *IEEE Transactions on Energy Conversion*, 36(4), pp. 2825–2838. Available at: https://doi.org/10.1109/tec.2021.3068174.

Smoleń (2018). Computationally efficient method for determining the most important electrical parameters of axial field permanent magnet machine. *Bulletin of the Polish Academy of Sciences: Technical Sciences - PAS Journals*, Available at: https://journals.pan.pl/dlibra/publication/125943/edition/109885/content.

Using Symmetry to Reduce Model Size (no date). Available at: https://www.comsol.com/support/learning-center/article/Using-Symmetry-to-Reduce-Model-Size-49411. (Accessed on January 18th 2023).

Van Der Giet, M., Schlensok, C., Schmulling, B. and Hameyer, K. (2008). Comparison of 2-D and 3-D Coupled Electromagnetic and Structure-Dynamic Simulation of Electrical Machines. *IEEE Transactions on Magnetics*, 44(6), pp. 1594–1597. Available at: https://doi.org/10.1109/tmag.2007.916121.